Journal of Thermal Analysis and Calorimetry, Vol. 90 (2007) 2, 475–488

EFFECT OF THERMAL DECOMPOSITION PROCESSES ON THE THERMAL PROPERTIES OF CARBON FIBER REINFORCED CEMENT COMPOSITES IN HIGH-TEMPERATURE RANGE

R. Černý[1*], *Jitka Němečková*[1], *Pavla Rovnaníková*[2] *and P. Bayer*[2]

[1]Department of Mechanics, Faculty of Civil Engineering, Czech Technical University, Thákurova 7, 166 29 Prague 6, Czech Republic
[2]Institute of Chemistry, Faculty of Civil Engineering, Brno University of Technology, Žižkova 17, 662 37 Brno, Czech Republic

Thermal conductivity, specific heat capacity, thermal diffusivity and linear thermal expansion coefficient of two types of carbon fiber reinforced cement composites are measured in the temperature range up to 800°C. Thermal conductivity and thermal diffusivity are also determined for the specimens exposed to thermal load up to 800°C before the measurement. Differential thermal analysis (DTA), mercury intrusion porosimetry (MIP), scanning electron microscopy (SEM) and X-ray diffraction analysis (XRD) are utilized for the assessment of thermal decomposition processes taking place in the high temperature range under consideration.

The high temperature thermal properties of the studied materials are found to be positively affected by the application of the high alumina cement and in the case of the Portland cement based composite also by using the autoclaving procedure in the production process. Also, the randomly distributed carbon fibers that can reduce the damage of the pore structure by the thermal decomposition processes are identified as a positive factor in this respect. A comparison of thermal conductivity *vs.* temperature curves obtained for the specimens pre-heated to different temperatures is found to be a useful tool in the identification of major dynamic effects in the specimens due to the thermal decomposition reactions. The results are in a good agreement with the DTA, MIP, SEM and XRD analyses. The character of the thermal conductivity measurements that in fact includes the effects of convection and radiation into the thermal conductivity coefficient can be beneficial for a simple assessment of the influence of the fire on a dividing structure.

Keywords: *carbon fiber reinforced cement composites, high temperatures, linear thermal expansion coefficient, specific heat capacity, thermal conductivity, thermal diffusivity*

Introduction

Carbon fiber reinforcement has found its application first in polymeric matrices for automotive and aircraft industry. It partially replaced previously used glass fibers in such situations where superior strength properties, very low tensile strains and mass savings were necessary. In the beginnings of carbon fiber production the most often used precursor was PAN (polyacrylonitrile) that gave superior carbon fiber properties but was quite expensive. The appearance of low cost pitch based carbon fibers in 1980s has led to a significant increase of various applications of carbon fibers. In the construction industry it resulted in an increasing use of carbon fiber reinforced cement composites (e.g., [1], for details). A comprehensive survey of both properties and processing of carbon fibers and of the various types of carbon fiber reinforced composites can be found in [2].

In the initial phases of development of carbon fiber reinforced cement composites (CFRC), their mechanical properties were in the center of interest of most researchers working on those materials because their main role was to improve the tensile and flexural strength of the cement matrix. A basic review of the measurements of mechanical properties, durability and dimensional stability of a variety of CFRC summarizing the research activities until 1977 was given in [3]. Later measurements of mechanical properties, particularly of specially developed new types of CFRC can be found e.g. in [4–7]. Aging of CFRC in terms of dependence of mechanical parameters on time was studied in [8].

Thermal properties of CFRC were measured only rarely until now. Thermal conductivity and specific heat capacity of CFRC at room temperature were studied in [9]. Any other measurements were not found by the authors in common sources.

As it has been mentioned earlier, CFRC can be potentially subject of similar applications as glass fiber reinforced cement composites. This also includes their application as thermal insulation materials in the range of elevated temperatures or fire protection materials. Here, the high temperature thermal properties such as thermal conductivity, thermal diffusivity specific heat capacity, linear thermal expansion coeffi-

* Author for correspondence: cernyr@fsv.cvut.cz

1388–6150/$20.00

Akadémiai Kiadó, Budapest, Hungary
Springer, Dordrecht, The Netherlands

cient are supposed to be measured to assess the protection function of an envelope in an appropriate way. However, there are not any references known to the authors dealing with the high-temperature thermal properties of CFRC. In such conditions any serious design of CFRC for elevated- and high-temperature applications does not seem to be possible.

Cement based materials in general were subject of high-temperature measurements of thermal parameters by various investigators within the several last decades. For instance, thermal expansion of cement paste in the temperature range to 800°C was measured in [10, 11], thermal expansion of various concretes up to 1000°C in [12, 13]. Specific heat capacity of cement paste was determined in [14], specific heat capacity of various types of concrete in [14, 15]. Thermal conductivity of cement paste was measured in [14], thermal conductivity of concrete in [12, 14, 15]. Thermal conductivity, specific heat capacity and linear thermal expansion coefficient of cement mortar up to 1000°C was studied in [17], thermal diffusivity and linear thermal expansion coefficient of several types of glass fiber reinforced cement composites up to 800°C in [18]. Thermal analysis of decomposition processes for cement paste was done in [19–22], for cement mortar in [23], for glass fiber reinforced cement composites in [18]. A more comprehensive survey of the thermal properties of concrete at high temperatures measured until approx. 1992 can be found in [24], a survey including more recent measurements in [25].

In this paper, thermal conductivity, specific heat capacity, thermal diffusivity and linear thermal expansion coefficient of two types of carbon fiber reinforced cement composites are determined in the temperature range up to 800°C.

Experimental

Methods for determination of thermal parameters in high temperature range

Specific heat capacity

As the adiabatic methods are not very suitable for measuring high-temperature specific heat capacity of building materials, mainly because of the necessity to use relatively large samples, a nonadiabatic method [26] was employed for the determination of temperature-dependent specific heat capacity. We will present the main idea of the method in what follows.

The nonadiabatic calorimeter has a mixing vessel with a volume of 2.5 L. The volume of the measuring fluid (water in this case) is about 1 L. The maximum volume of the measured samples is 1 L. The amount of heat loss of the non-adiabatic system is determined using a calibration. The calorimeter is filled with water, whose temperature is different from the ambient air. Then, the relation of water temperature to time, $T_c(t)$, is measured.

The measuring method itself is based on well-known principles. The sample is heated to a predetermined temperature T_s in a furnace and then put into the calorimeter with water. Then, the relation of water temperature to time $T_w(t)$ is measured, water being slowly stirred all the time, until the temperatures of the measured sample and the calorimeter are equal. The corrected (adiabatic) temperature $T_r(t)$ taking the heat loss into account is calculated using the corrections $\Delta T(t_i)$ obtained from the calibration curve $T_c(t)$,

$$T_r(t_i) = T_w(t_i) + \Delta T(t_i) \quad (1)$$

where

$$\Delta T(t_i) = \sum_{j=1}^{i} \Delta T(t_j) \quad (2)$$

$$t_i = \sum_{j=1}^{i} \Delta t_j \quad (3)$$

The theoretical equilibrated temperature of the sample-calorimeter system at the end of the test T_e is then calculated as

$$T_e = \lim_{t \to \infty} T_r(t) \quad (4)$$

The heat balance of the sample-calorimeter system can be written in the form:

$$mc(T_s - T_e) = (K + m_w c_w)(T_e - T_{wo}) + \Delta mL - Q_r \quad (5)$$

where m is the mass of the sample, c is the specific heat capacity of the sample in the temperature interval $[T_e, T_s]$, K is the heat capacity of the calorimeter, m_w is the mass of the water, c_w is the specific heat capacity of water, T_{wo} is the initial water temperature, L is the latent heat of evaporation of water, Q_r is the reaction heat, Δm is the mass of evaporated water,

$$\Delta m = m + m_{cw} - m_s - \Delta m_N - \Delta m_{sc} \quad (6)$$

m_{cw} is the mass of the calorimeter with water before the measurement, m_s is the mass of the system calorimeter-water-sample after measurement, Δm_N is the mass of water, naturally evaporated during the measurement (this heat loss is already included in the heat loss calibration curve), Δm_{sc} is the change of mass due to the chemical reaction of the sample with water (e.g., hydrolysis). This value can be obtained as $\Delta m_{sc} = m - m_D$, where m_D is the mass of the dried sample after the measurement. The remaining symbols in Eq. (5) are the same as before.

Determining the specific heat capacity c directly from Eq. (5) we would obtain a mean value of the specific heat capacity, c_0, in the interval $[T_e, T_s]$ by

$$c_0=\frac{(K+m_w c_w)(T_e-T_{wo})+\Delta mL-Q_r}{m(T_S-T_e)} \quad (7)$$

However, from the physical point of view, it is more correct to determine the value of the specific heat capacity 'point-wise', in accordance with the definition of specific heat capacity,

$$c(T_i)=\frac{\partial h}{\partial T}(T_i) \quad (8)$$

where h is the specific enthalpy.

Using relation (8) to determine the specific heat capacity, we have to specify the zero-point of the enthalpy scale, i.e., we have to ensure that all the enthalpy calculations are related to a certain constant temperature. This reference temperature can be, for example, T_k=0°C. Upon adding

$$Q=mc_e(T_e-T_k) \quad (9)$$

where c_e is the mean specific heat capacity of the sample in the temperature interval $[0,T_e]$, to both sides of Eq. (5), and dividing by m, we obtain the following

$$h(T_s)=\frac{(K+m_w c_w)(T_e-T_{wo})+\Delta mL-Q_r}{m}+c_e(T_e-T_k) \quad (10)$$

The value of c_e is considered to be constant, taking into account the condition

$$T_s-T_e>>T_e-T_k \quad (11)$$

and it can be measured, for example, using the classical adiabatic method.

Performing a set of measurements for various sample temperatures T_i, we obtain a set of points $[T_i,h(T_i)]$. A regression analysis of this point-wise given function results in a functional relationship for $h=h(T)$ and, using relation (8), also in the function $c=c(T)$ as the first derivative of h with respect to T.

Thermal conductivity

For the determination of high-temperature thermal conductivity we used the double integration method [27], a dynamic method based on an inverse analysis of the temperature field.

The basic principle of the method consists in measuring the temperature field $T(x,t)$ in the sample at one-sided heating and the subsequent solution of the inverse heat conduction problem. We suppose $T(t)$ and $T(x)$ to be monotonic functions and choose a constant value of temperature, $\tau=T(x,t)$. Then must exist one-to-one parametrizations $x=x_0(\tau,t)$, $t=t_0(\tau,x)$ where both x_0 and t_0 are monotonic functions. Considering this fact, an integration of heat conduction equation by x and t leads to

$$\int_{t_1}^{t_n}\int_{0}^{x_0(\tau,t)}\rho c\frac{\partial T}{\partial t}\mathrm{d}x\mathrm{d}t= \\ =\lambda(\tau)\int_{t_1}^{t_n}\frac{\partial T}{\partial x}(x_0(\tau,t),t)\mathrm{d}t-\int_{t_1}^{t_n}\lambda[T(0,t)]\frac{\partial T}{\partial x}(0,t)\mathrm{d}t \quad (12)$$

where

$$-\lambda[T(0,t)]\frac{\partial T}{\partial x}(0,t)=j_Q(0,t) \quad (13)$$

is the heat flux at x=0.

The left-hand side (LS) of Eq. (12) can be modified by accounting for the shape of the integration area:

$$LS=\int_{t_1}^{t_n}\int_{0}^{x_0(\tau,t)}\rho c\frac{\partial T}{\partial t}\mathrm{d}x\mathrm{d}t= \\ \int_{0}^{x_0(\tau,t_1)}\mathrm{d}x\int_{t_1}^{t_n}\rho c\frac{\partial T}{\partial t}\mathrm{d}t+\int_{x_0(\tau,t_1)}^{x_0(\tau,t_n)}\mathrm{d}x\int_{t_0(\tau,x)}^{t_n}\rho c\frac{\partial T}{\partial t}\mathrm{d}t \quad (14)$$

Denoting

$$\int\rho c\frac{\partial T}{\partial t}\mathrm{d}t=\int\rho(T)c(T)\mathrm{d}T=I_T(T) \quad (15)$$

we obtain

$$LS=\int_{0}^{x_0(\tau,t_1)}[I_T(T(x,t_n))-I_T(T(x,t_1))]\mathrm{d}x+\int_{x_0(\tau,t_1)}^{x_0(\tau,t_n)}[I_T(T(x,t_n))-I_T(\tau)]\mathrm{d}x= \\ =\int_{0}^{x_0(\tau,t_n)}[I_T(T(x,t_n))\mathrm{d}x-\int_{0}^{x_0(\tau,t_1)}I_T(T(x,t_1))\mathrm{d}x-I_T(\tau)[x_0(\tau,t_n)-x_0(\tau,t_1)] \quad (16)$$

Substituting (16) into (12) we arrive at

$$\lambda(\tau)=\frac{\int_{0}^{x_0(\tau,t_n)}I_T(T(x,t_n))\mathrm{d}x-\int_{0}^{x_0(\tau,t_1)}I_T(T(x,t_1))\mathrm{d}x-I_T(\tau)[x_0(\tau,t_n)-x_0(\tau,t_1)]-\int_{t_1}^{t_n}j_Q(0,t)\mathrm{d}t}{\int_{t_1}^{t_n}\frac{\partial T}{\partial x}(x_0(\tau,t),t)\mathrm{d}t)} \quad (17)$$

where for $t_j > t_i$ the heat flux at $x=0$ can be calculated as

$$j_Q\left(0,\frac{t_j+t_i}{2}\right)= \\ =\frac{1}{t_j-t_i}\int_0^D[\rho(T)c(T)T(x,t_j)-\rho(t)c(T)T(x,t_i)]\mathrm{d}x \quad (18)$$

where D is the length of the one-dimensional domain under consideration.

The measuring procedure consists then in the following. One-side heating of a specimen (for cement based materials typically 71×71×71 mm) with thermally insulated lateral faces is realized using a furnace where a constant temperature is maintained. Along the longitudinal axis of the sample, a set of temperature sensors is positioned, which makes it possible to record the temperature field through a measuring unit by a PC. From the measured $T(x,t_i)$ curves, a set of 8–10 curves is chosen, and these curves are used in the computational treatment. First, the measured $T(x,t_i)$ curves are subject of a regression analysis. Then, we choose a temperature value τ, determine the integration area for this value and calculate the corresponding value of thermal conductivity $\lambda(\tau)$ by Eq. (17). This procedure is repeated for a sufficient number of τ values so that we finally obtain a point-wise given function $[\tau_i,\lambda(\tau_i)]$.

Thermal diffusivity

The high-temperature thermal diffusivity was calculated from its definition formula

$$a(T)=\frac{\lambda(T)}{\rho(T)c(T)} \quad (19)$$

in the paper.

Linear thermal expansion coefficient

In measuring the high-temperature linear thermal expansion coefficient, the method proposed in [28] was employed. The measuring device (the extensometer) consists of a cylindrical, vertically oriented electric furnace with two bar samples placed in the furnace. The first sample is the measured material, the second sample is a reference material for which the dependence of thermal expansion coefficient on temperature is known. The length changes of the samples are measured mechanically by dial gauges outside the furnace using thin ceramic rods that pass through the furnace cover and are fixed on the top of the measured sample. These ceramic rods pass through an undefined temperature field, so their normal strain cannot be determined mathematically, and a comparative method of determining the normal strain of the rod is used instead.

A practical measurement of the linear thermal expansion coefficient of a building material using the extensometer from [28] can be described as follows. The measured sample and the standard are put into the furnace, fitted with the contact ceramic rods, and the initial reading on the dial gauges is taken. The furnace control system is then adjusted to the desired temperature T_i, the length changes are continuously monitored on the dial gauges and recorded by a computer. After the steady state is achieved, i.e. no temperature changes in the furnace and no length changes of both measured sample and the standard are observed, the final readings of length changes are taken. The length change of the measured sample is calculated according to the formula

$$\Delta l(T_i)=\Delta l_m(T_i)-\Delta l_s(T_i)+l_{0,s}\int_{T_0}^{T_i}\alpha_s(T)\mathrm{d}T \quad (20)$$

where Δl_m, Δl_s are the final readings of total length changes of the measured sample and of the standard, respectively, including the length changes of the ceramic rods, $l_{0,s}$ is the initial length of the standard, and $\alpha_s(T)$ is the known linear thermal expansion coefficient of the standard.

The corresponding value of normal strain can be expressed in the form

$$\varepsilon(T_i)=\frac{\Delta l(T_i)}{l_{0,m}} \quad (21)$$

where $l_{0,m}$ is the initial length of the measured sample.

The measurements are then repeated with other chosen values of furnace temperatures T_i, the point-wise function $[T_i,\varepsilon(T_i)]$ is obtained, which is then subject of a regression analysis. The linear thermal expansion coefficient α is then determined according to the definition relation

$$\alpha(T)=\frac{\partial\varepsilon(T)}{\partial T} \quad (22)$$

Materials and samples

The carbon fiber reinforced cement composite specimens (denoted as CC I and CC III) had the composition shown in Table 1 (the percentage is calculated among the dry substances only). Portland cement CEM I 52.5 Mokrá was used for CC I, high alumina cement Alcoa CA-14M for CC III, carbon fiber was pitch based with 10 mm length. Water in the amount corresponding to the w/c ratio of 0.8 was added to the mixture for CC I, 0.73 for CC III.

The samples were produced in the laboratories of VUSTAH, SA (CZ) using a successive homogenization procedure. First, wollastonite, microdorsilite and microsilica were homogenized in a mixing de-

Table 1 Composition of carbon fiber reinforced cement composites in % of dry substances

	Cement	Micro-dorsilite	Plasti-cizer	Carbon fiber	Wolla-stonite	Methyl-cellulose	Defoamer	Microsilica
CC I	39.71	16.50	0.98	0.98	39.60	0.11	0.16	1.96
CC III	40.00	28.40	0.80	1.00	29.50	0.10	0.20	–

vice, then cement and methylcellulose were added and the dry mixture was homogenized again. The dry well homogenized mixture was thoroughly mixed with water, defoamer and plasticizer. Then, the carbon fibers were added and the mixture shortly mixed again. Finally, the prepared mixture was vacuum-treated in special molds with perforated bottom. The material CC I was autoclaved at 180 and then dried at 105°C, the material CC III was cured in common way. After the time period of 28 days after mixing, the samples were prepared for testing.

The dimensions of the specimens for determination of specific heat capacity and thermal conductivity were 71×71×71 mm, for the linear thermal expansion coefficient measurements 40×40×100 mm. We used 10 specimens for measurements of the specific heat capacity, 5 specimens for measurements of the thermal conductivity and 10 specimens for measuring the linear thermal expansion coefficient.

For the measurements of thermal conductivity, two different specimen pre-treatment conditions were analyzed: reference specimen not exposed to any thermal load and specimen exposed to the temperatures of 200, 400, 600 and 800°C. Heating of the specimens to the pre-treatment temperature was always done with the rate of 10 K min^{-1}, then the specimens remained at that temperature for the time period of two hours, and finally they were cooled with the rate of 2 K min^{-1}.

In the measurements of thermal conductivity of both reference specimens and thermally pre-treated specimens, the furnace was first preheated to the chosen temperature for two hours to achieve thermal homogenization. Then the specimens that were kept at room temperature until this moment were subjected to a thermal shock from one side and the experiment continued as described in 'Thermal conductivity'.

In the measurements of specific heat capacity and linear thermal expansion coefficient the thermal pre-treatment was not applied because it would not have much sense – the measuring methods are in fact steady-state methods and the specimens are thermally homogenized at each measuring temperature. Heating of the samples to the chosen temperature was done in both methods with the rate of 10 K min^{-1}. The thermal conditions in the furnaces were homogenized in the same way as with the measurements of thermal conductivity.

Results and discussion

Basic room-temperature properties

Table 2 shows the basic room-temperature properties of the studied carbon fiber reinforced cement composites that were determined for the sake of comparison with the high-temperature data. The thermal conductivity λ was measured using the impulse technique (commercial device ISOMET 2104, Applied Precision), the specific heat capacity c using a common mixing calorimeter, the bulk density ρ by measuring the dimensions of the samples and weighing, the thermal diffusivity a was calculated from the values of λ, c and ρ.

Table 2 Basic properties of carbon fiber reinforced cement composites – room temperature values

Property	CC I	CC III
Bulk density/kg m^{-3}	1545	1595
Thermal conductivity/W m^{-1} K^{-1}	0.62	1.132
Specific heat capacity/J kg^{-1} K^{-1}	985	1020
Thermal diffusivity/10^{-6} m^2 s^{-1}	0.407	0.696

There is one point worth commenting on the room-temperature properties in Table 2. Although the bulk density of the material CC I is only by about 3% lower compared to CC III, its thermal conductivity is lower by almost 50%. The reason for this unusual combination of properties might be the more homogeneous pore structure of CC I achieved by autoclaving. Therefore, characterization experiments by mercury intrusion porosimetry (MIP) were performed on both materials.

Mercury porosimetry

The results of MIP measurements in Figs 1a and b show that while the total intrusion volume for the reference specimens is almost the same for both materials, the distribution of pores is very different. The material CC I clearly has the majority of pores between 10 and 100 nm, contrary to CC III where the majority of pores is between 500 nm and 2 μm. Therefore, we have a good reason to believe that the finer pore structure of CC I results in a more homogeneous pore distribution compared to CC III. Concerning the thermal conductivity, the more homogeneous pore structure in CC I probably had led to the relative increase of the effect of air voids in the material on its heat transport

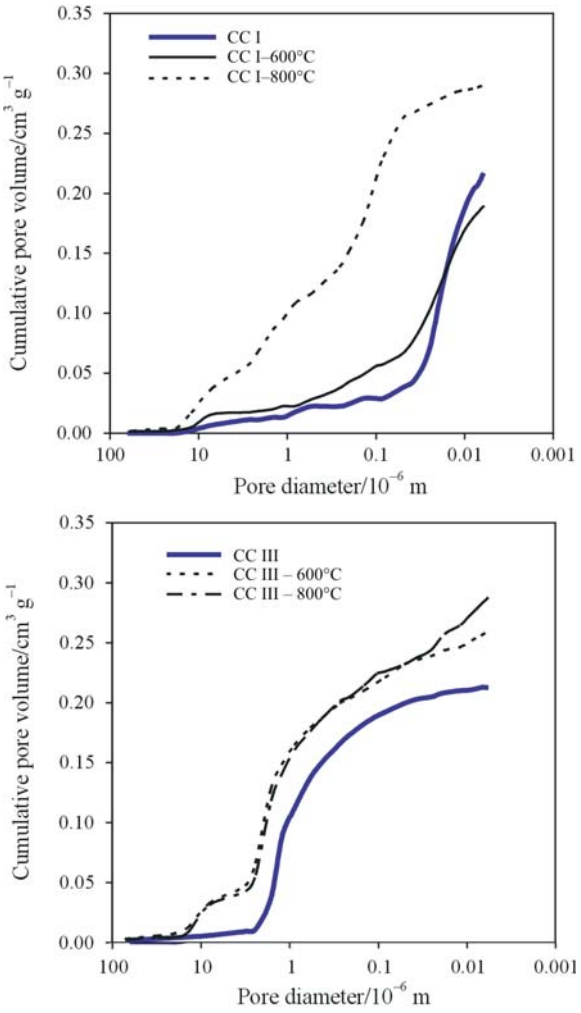

Fig. 1 Cumulative pore volume of carbon fiber reinforced cement composites CC I, CC III

related macroscopic properties while in CC III the presence of significantly bigger pores could result in a formation of thermal bridges in the structure accompanied by an increase in thermal conductivity.

High-temperature bulk density

Before the determination of high-temperature thermal properties, the bulk density as function of temperature had to be measured in the chosen high-temperature range because it appears as one of the necessary parameters for the determination of high-temperature thermal conductivity (Eq. (17)). The measurements were done on large specimens (71·71·71 mm) by measuring the dimensions of the samples and weighing.

Figure 2 shows that the dependence of bulk density of the material CC I was almost uniformly decreasing without any dramatic changes. This is a remarkably different behavior in comparison with the thermogravimetric curve of cement mortar obtained by classical thermal analysis using the Derivatograph device before ([29]) where the irregularities corresponding to the decomposition of $Ca(OH)_2$ and $CaCO_3$ were very distinct. The character of the bulk density *vs.* temperature curve of the material CC III was much more dramatic compared to CC I. A fast decrease was observed between 200 and 400°C while the other parts of the curve were almost flat.

DTA, XRD and SEM experiments

As the bulk density measurements revealed a not very common behavior of both materials in the range of higher temperatures, more thorough thermal analysis measurements were done on both CC I and CC III using the derivatograph device in the same way as in [29].

At the hydrothermal reaction of cement with water the metastable phase $C_6S_2H_3$ is formed first that is decomposed later. The original CSH gels are converted to C_2SH as the main phase and the aluminous phase hydrates to the final product C_3AH_6.

Figure 3 presents the DTA curve of the material CC I. The first dip between 100 and 200°C (corresponding to an endothermic process) can be attributed to the decomposition of C_2SH and of the aluminous phase. The burning-out of pitch-based carbon fibers begins at the temperature of 480°C. The lubrication burns first and the fiber itself burns-out in the temperature range between 600 and 800°C. This is documented in more detail in Fig. 4 where the thermal degradation of separated pitch-based carbon fibers is presented. Coming back to Fig. 3, there is one more important feature on the DTA curve. At the temperature of 850°C, there is a distinct exothermic peak corresponding to the reaction of products of the C_2SH decomposition with silicon dioxide (microdorsilite and microsilica) resulting in the formation of

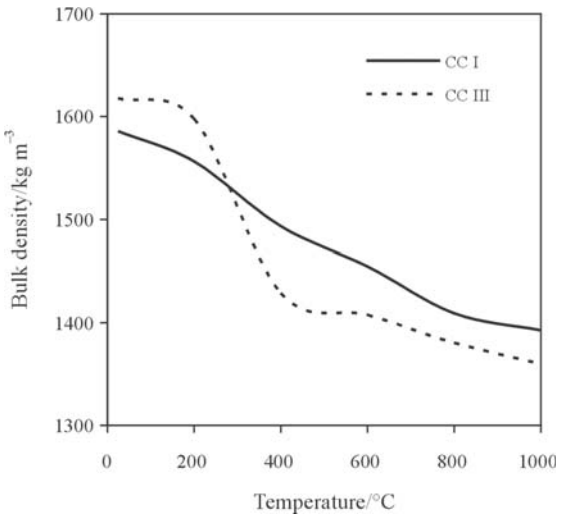

Fig. 2 Bulk density of carbon fiber reinforced cement composites CC I, CC III

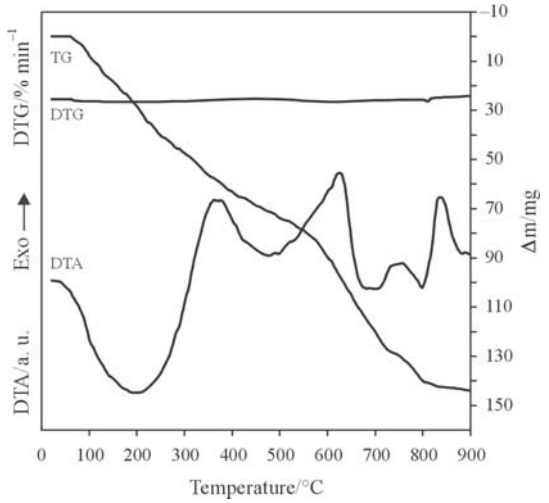

Fig. 3 Thermal analysis of the carbon fiber reinforced cement composite CC I

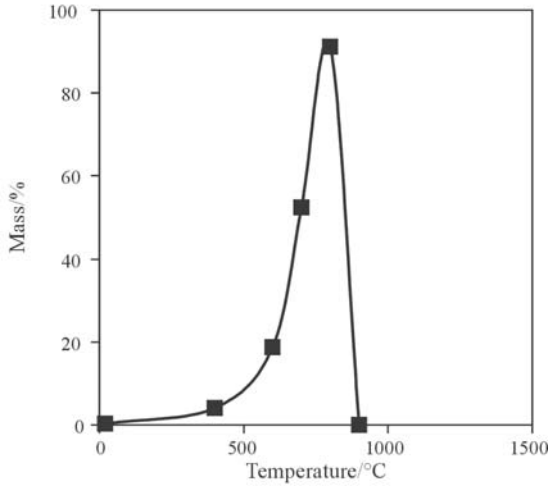

Fig. 4 Thermal degradation of pitch-based carbon fiber

wollastonite. The TG curve in Fig. 3 corresponds to the DTA findings and further illustrates the successive decomposition of the hydrated phases of cement and the carbon fiber burning-out. The total mass loss is 14.3%, which is in a reasonable agreement with the measurements of bulk density in Fig. 2 where it was 12.1%.

As it follows from the above interpretation of Fig. 3, the autoclaving process has changed the phase composition of the Portland cement based composite CC I in quite a significant way. Therefore, some additional characterization experiments were done.

The X-ray diffraction (XRD) analysis of the material CC I before heating in Fig. 5a showed the presence of tobermorite (T), quartz (Q) and wollastonite (W). After heating to 600°C (Fig. 5b), the content of the tobermoritic phase was decreased. Heating to 1000°C (Fig. 5c) then led to a complete loss of tobermorite while the quartz and wollastonite were preserved.

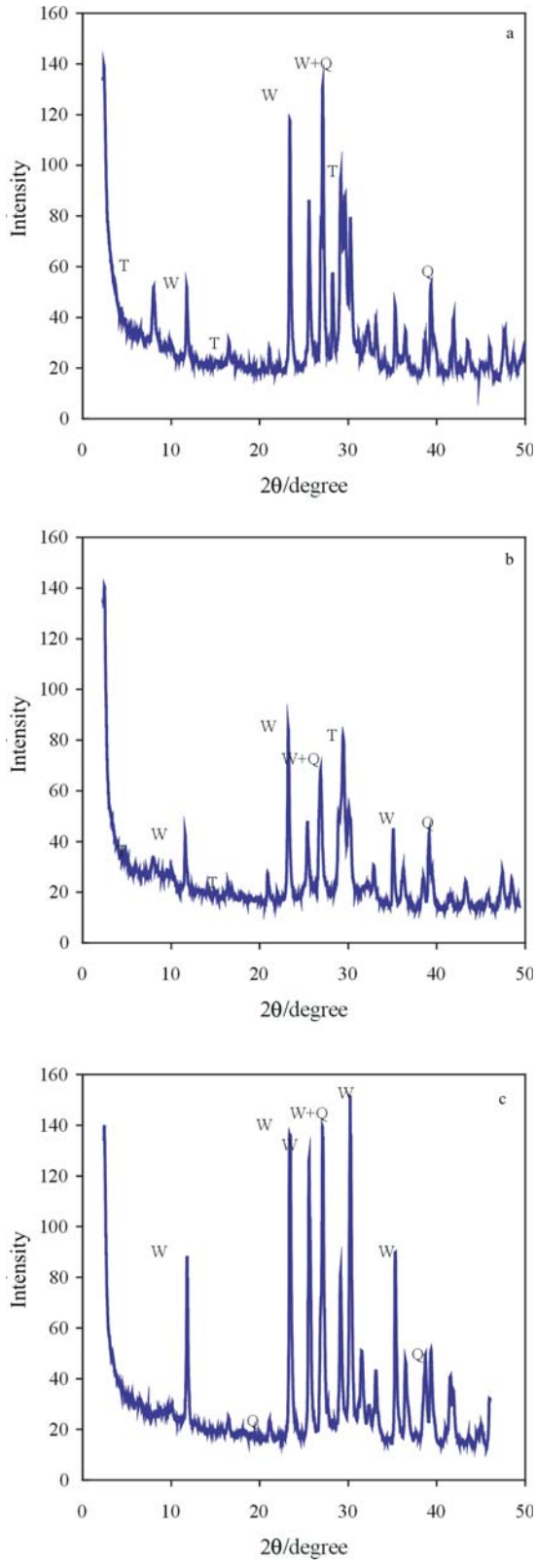

Fig. 5 X-ray diffraction analysis of CCI at a – normal laboratory temperature, b – after loading to the temperature 600°C, c – after loading to the temperature 1000°C

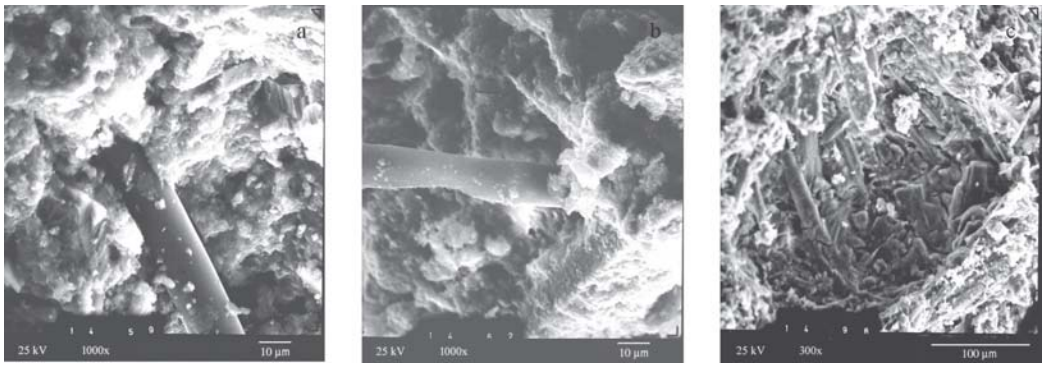

Fig. 6 Scanning micrographs of CC I sample at a – 20, b – 600 and c – 1000°C

SEM images in Figs 6a–c show that after heating the CC I sample to 600°C for 1 h the fibers already were seriously damaged, for 1000°C heating the fibers were missing at all due to their burning-out. This is in a reasonable agreement with the results of DTA measurements in Figs 3 and 4. However, it should be noted in this respect that DTA analysis itself can not detect the exact temperature of fiber burning-out because the air is in full contact with the fibers during a DTA experiment. In a real material the cement matrix is supposed to protect the fibers against the contact with the air to a certain extent.

The DTA curve of the material CC III in Fig. 7 shows that the hydration product of the high alumina cement was just C_3AH_6, that was then decomposed at the temperature of about 300°C. In order to separate the effect of the high alumina cement ALCOA CA-14 M itself from the possible effects of other components, another DTA analysis was done for high alumina cement paste (w/c=0.5, 28 days after mixing). The results are presented in Fig. 8. The endothermal delay in the temperature range of 130 to 150°C corresponds to the decomposition of AH_3 and CAH_{10}. Also, a small amount of C_2AH_8 is noticeable on the DTA curve. We note that both the metastable phases CAH_{10} and C_2AH_8 are missing on the DTA curve of CC III in Fig. 7. The apparent reason for this fact is their conversion to C_3AH_6. The second endothermal peak at 305°C in Fig. 8 corresponds to the decomposition of C_3AH_6. The high alumina cement paste was not carbonated. So, no endothermal peak corresponding to the decomposition of calcium carbonate appeared. The exothermal delay at the temperature of 920°C without any mass loss on the TG curve in Fig. 8 is due to the crystallization of Al_2O_3. The total mass loss was for the high alumina cement paste 21.2%.

Coming back to the DTA curve of the material CC III in Fig. 7, we can realize that the pitch based carbon fibers start to burn out from the temperature of 560°C. The end of the fiber burning out is not noticeable because the exothermal delay is mixed with the decomposition of calcium carbonate that was formed due to the reaction with carbon dioxide in the air. This decomposition begins at the temperature of 770°C, with a minimum at 825°C. The total mass loss was for the material CC III 16.5%.

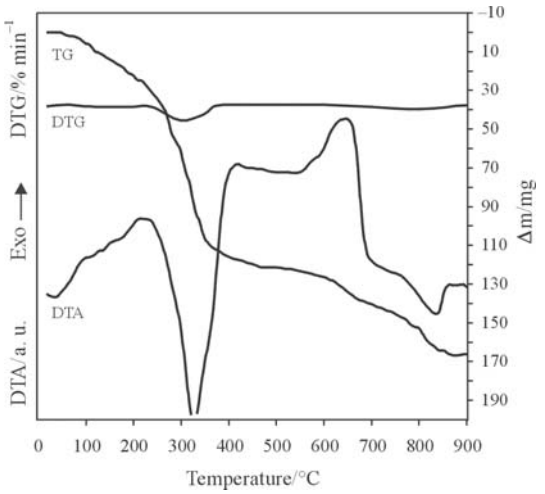

Fig. 7 TG DTG and DTA curves of the carbon fiber reinforced cement composite CC III

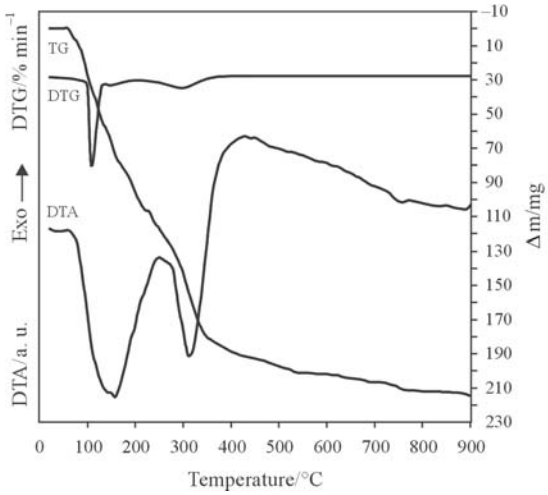

Fig. 8 TG DTG and DTA curves of the high alumina cement paste

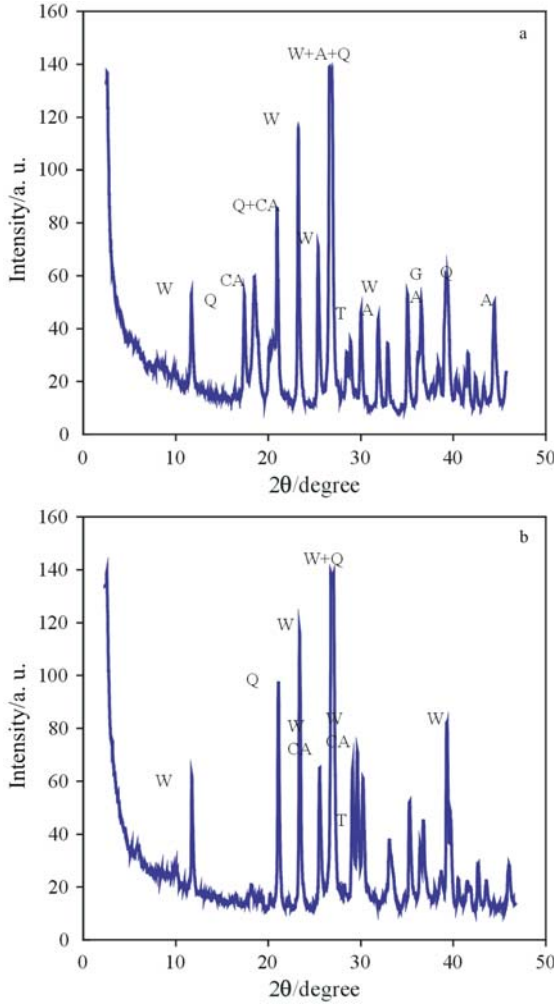

Fig 9 X-ray diffraction analysis of the material CC III at a – normal laboratory temperature, b – after loading at the temperature 600°C

The X-ray diffraction analysis of the CC III sample before heating in Fig. 9a revealed the appearance of C_3AH_6 (A), the remainders of non-hydrated cement CA, CA_2, $C_{12}A_7$ (CA), silica, wollastonite and gehlenithydrate (G). The X-ray analysis of CC III after heating to 600°C in Fig. 9b shows only the appearance of silica, wollastonite and anhydrous calcium aluminates.

SEM images in Figs 10a–c show that in the CC III material the carbon fiber had after heating to 600°C smaller diameter, and even some pores due to fiber burning out appeared. The solitary straw-like formations in Fig. 10c corresponding to the sample heated to 1000°C present wollastonite.

Summarizing the results of the analysis of fiber burning out obtained by DTA, mercury porosimetry and SEM analyses we can conclude that the autoclaved Portland cement composite presented a better protection to the air penetration to the fibers than the high alumina cement composite where higher cumulative pore volume was found.

High-temperature specific heat capacity

Figure 11 shows the high-temperature specific heat capacity of both studied materials. We can see that the $c(T)$ curve of the material CC I exhibits slightly decreasing character and for 800°C it is about 10% lower than in room temperature conditions. The character of the $c(T)$ curve of CC III is different, it increases first up to about 500°C, in maximum it is approximately 20% higher than at room temperature, and then decreases so that for 800°C it achieves the value of about 10% lower than at room temperature. So, the changes of the specific heat capacity are in absolute numbers not very dramatic. Taking into account the error range of the method to be about ±10% ([26]), we can conclude that the measured dependence of the specific heat capacity on temperature was very close to the accuracy limit of the method.

High-temperature thermal conductivity

Figures 12a and b show that the high-temperature thermal conductivities of both CFRCs appear to depend on temperature in much more significant way than the specific heat capacities. The measured differences are well outside the error range of the measuring method in this case. Also, the thermal pre-treatment of the samples was found to be a very significant

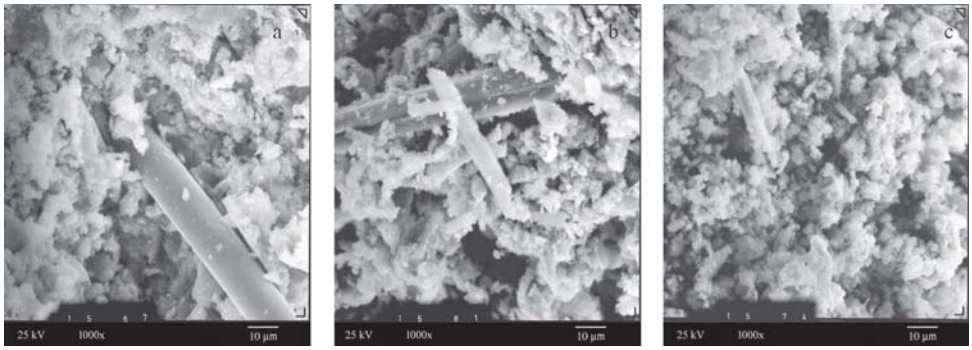

Fig. 10 Scanning micrographs of CC III sample at a – 20, b – 600 and c – 1000°C

factor affecting both the shape of the $\lambda(T)$ curves and the magnitude of the thermal conductivity values.

The basic $\lambda(T)$ function (samples without any thermal pre-treatment) of the material CC I exhibits an increase of thermal conductivity with temperature up to about 330°C where the λ value is about two times higher than at 150°C, and then the thermal conductivity begins to decrease so that at 800°C the λ value is approximately the same as at 150°C. This basic character of the $\lambda(T)$ functions remains the same for all the samples with thermal pre-treatment as well. However, the magnitudes of the λ values are changed and also the positions of the λ maxima are shifted compared to the basic $\lambda(T)$ function of the samples without any thermal pre-treatment.

The $\lambda(T)$ function of CC I corresponding to the 200°C pre-heating is only moderately shifted above the basic $\lambda(T)$ function. Its maximum is at about 350°C and 20% higher. The 400°C pre-heating $\lambda(T)$ function exhibits differences much higher. The maximum of the function is at 460°C and is almost two times higher than that of the basic $\lambda(T)$ function. The $\lambda(T)$ function corresponding to the 600°C pre-heating has its maximum at 430°C. It is about 20% lower than the maximum of the 400°C pre-heating $\lambda(T)$ function. For the temperatures higher than approximately 600°C this function achieves the highest values among all $\lambda(T)$ functions of CC I, almost two times higher than the basic function. The 800°C pre-heating $\lambda(T)$ function is found to be the closest to the basic $\lambda(T)$ function. Its maximum is at almost exactly the same position and only 20% higher. In the range of temperatures higher than 500°C both functions almost coincide.

The basic character of $\lambda(T)$ functions remains unchanged also for the material CC III, i.e. the functions have just one maximum. The magnitude of changes of thermal conductivity and also the effect of

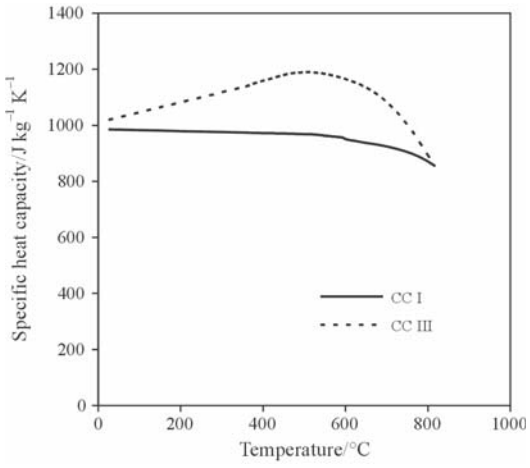

Fig. 11 Specific heat capacity of carbon fiber reinforced cement composites CC I, CC III

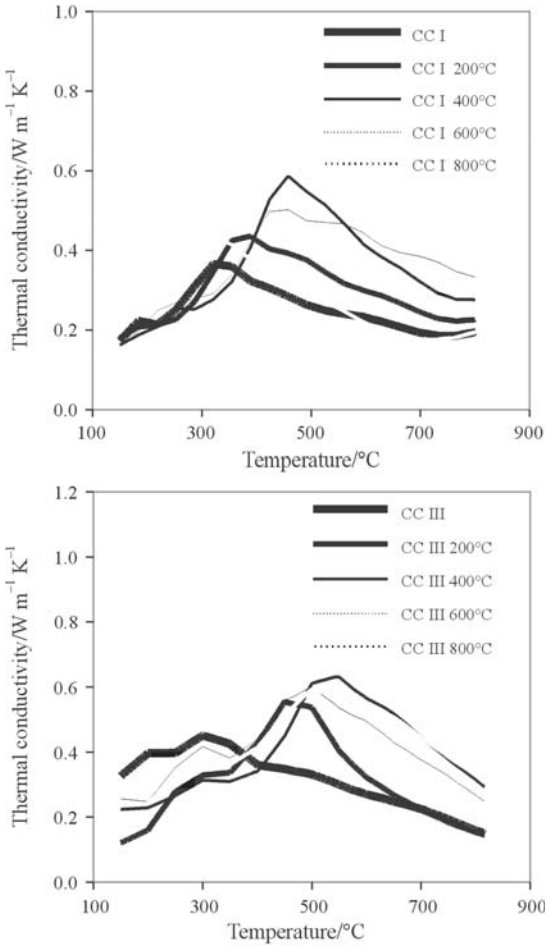

Fig. 12 Thermal conductivity of carbon fiber reinforced cement composites CC I, CC III as a function of thermal load

the particular pre-heating temperatures is different compared to CCI. Already the basic $\lambda(T)$ function differs from that of CC I. The increase up to 300°C is slower (about 30%) and the subsequent decrease faster (at 800°C the λ value is equal to about one half of that at 150°C) in comparison with CC I.

Contrary to CC I, already the 200°C pre-heating $\lambda(T)$ function of CC III exhibits very significant differences compared to the basic function. The maximum is shifted to 450°C and is approximately 25% higher. Also, in the lower temperature range up to about 400°C the λ values are down to two times lower. The $\lambda(T)$ functions of CC III corresponding to the 400, 600 and 800°C pre-heating have very similar courses but they are different from the former two functions. The λ values in the lower temperature range up to about 400°C are lower than the basic function of the thermally untreated material but higher than the $\lambda(T)$ function corresponding to the 200°C pre-heating. The λ maxima are shifted to 500–550°C and they are higher by only about 10% than at the 200°C pre-heating $\lambda(T)$ function. For the temperatures higher than approximately 500°C, the

$\lambda(T)$ functions corresponding to the 400, 600 and 800°C pre-heating achieve up to about two times higher values than the basic $\lambda(T)$ function and the 200°C pre-heating function.

The remarkable changes in the $\lambda(T)$ functions calculated using an inverse analysis of measured temperature fields have their origin in two fundamental factors. The first of them is that the measurements are dynamic. The temperature fields are measured typically for only about 30 min because one of the limiting conditions of the applied inverse analysis method is that the heat flux at the end of the sample not being in contact with the hot environment of the furnace should be equal to zero. Therefore, all chemical decomposition processes and phase change processes taking place at elevated temperatures affect the measurements in a very significant way. These processes are mostly endothermal so that they consume certain amount of heat that otherwise would be transported in the direction of the decreasing temperature. This leads to the appearance of disturbances in temperature gradients in the vicinity of places where the particular chemical reaction or the particular phase change process takes place.

The second important factor influencing the calculated $\lambda(T)$ functions is convection and radiation effects in the high temperature range. In the experimental setup applied for measurements where the temperature gradients exist in the whole volume of the sample these effects cannot be avoided. Therefore, the thermal conductivity determined in our experiment is not the classical Fourier thermal conductivity as in the most of other methods but generalized or apparent thermal conductivity that includes in certain extent also other modes of heat transfer. This fact could be beneficial for the practice in some cases. For instance, in the assessment of the influence of a fire on a dividing structure or in any other case where one-sided heating occurs this apparent thermal conductivity can be conveniently used instead of the common thermal conductivity coefficient exactly in the same way.

The thermal pre-treatment that was done for a part of specimens in this paper can help to distinguish between the purely dynamic effects caused by the immediate chemical reactions or phase change processes and the persistent effects arising from the fact that the thermal conductivity of the original material has to be different from the material where the above processes are already completed and which in fact already becomes a new material different from the original one.

As for the material CC I containing Portland cement, after the 800°C pre-heating the major decomposition processes are supposed to be completed (see the results of DTA analysis in Fig. 3). The comparison of the basic $\lambda(T)$ function and the 800°C pre-heating function shows only differences in the range of lower temperatures. This may indicate that the products of the decomposition reactions have higher apparent thermal conductivity than the original material.

In the material CC III the major decomposition processes should be completed already after 400°C pre-heating (Fig. 7). This is reflected well in our thermal conductivity measurements where the differences between the $\lambda(T)$ functions corresponding to the 400, 600 and 800°C pre-heating were found to be relatively small. However, the character of differences between the basic $\lambda(T)$ function and the 400°C pre-heating function is for CC III quite different than for CC I. The apparent thermal conductivity after completion of decomposition reactions is in the lower temperature range lower and in the higher temperature range higher than for the original material.

As it follows from the thermal analysis measurements, the decomposition processes in cement binder are for the studied materials the major factor affecting the changes in the porous structure induced by high temperatures. The aggregates used in the production of both materials, namely wollastonite, microdorsilite and microsilica can resist very well to high temperatures. Therefore, the different thermal behavior of both studied materials in both high-temperature range and after pre-heating expressed by the differences in thermal conductivities is apparently related to the quite different types of cement used in CC I and CC III production.

The changes in apparent thermal conductivity due to the changes in the pore size and pore distribution have – contrary to the Fourier thermal conductivity – an ambiguous character. The presence of bigger pores should generally lead to a decrease in heat conduction. On the other hand, the effects of convection and radiation enhance the heat transfer in the material and therefore increase the apparent thermal conductivity. These effects should be more important again in the materials with bigger pores where due to the higher temperature gradients the mutual radiation between the pore walls is more intensive and the convective motion of the air can achieve higher velocities. So, it is the balancing between these two contradictory factors that decides about the total change in apparent thermal conductivity after the high-temperature induced structural changes.

The effects of convection and radiation should generally be more distinct in the range of higher temperatures because the radiated energy increases with the fourth power of absolute temperature and both convection and mutual radiation are affected by the temperature gradient that is in our experimental setup significantly higher in the parts of the samples with higher temperatures. However, the real significance

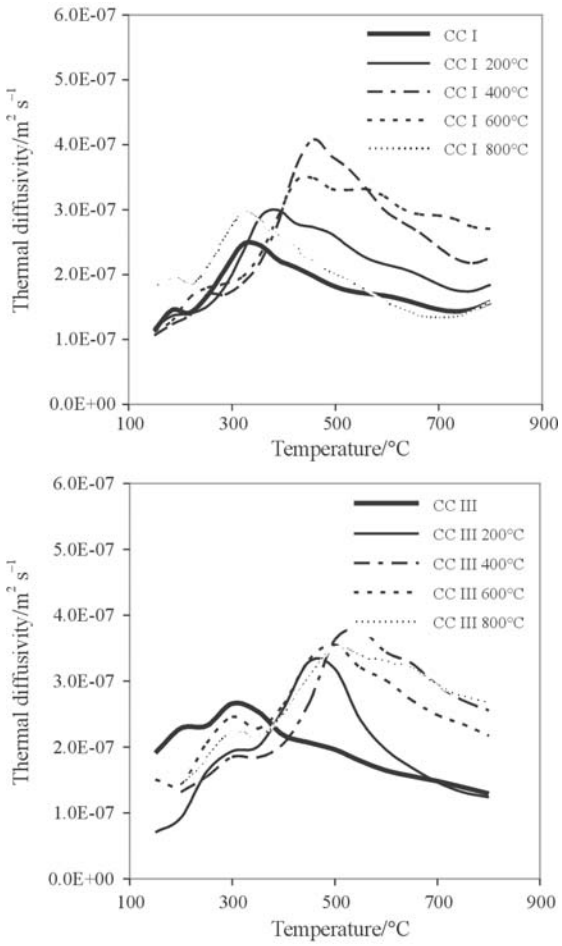

Fig. 13 Thermal diffusivity of carbon fiber reinforced cement composites CC I, CC III as a function of thermal load

of this effect should depend again on the pore size and pore distribution, which affect the balancing between the conductive heat transfer on one side and convective and radiative heat transfer on the other.

Thermal conductivity vs. pore structure correlation

In order to assess the possible correlation between the thermal conductivity and the pore structure in the above sense, we measured the cumulative pore volume of the materials CC I, CC III pre-heated to 600 and 800°C. The results are presented in Figs 1a and b.

As for the material CC I, after the 600°C pre-heating we observe only minor increase of the amount of bigger pores while the total pore volume slightly decreases in a comparison to the reference curve. Therefore, we suppose that the main reason for the relatively large difference in thermal conductivity for these two particular cases were the dynamic effects. The situation with the 800°C pre-heating was already very different. The amount of pores remarkably increased in the relatively wide range of about 100 nm–5 μm and the total pore volume increased by about 50%. In the upper part of this pore dimension interval the convective effects should already be distinct, the increase in total pore volume in turn should decrease the Fourier thermal conductivity. As the course of thermal conductivity with temperature was similar for these two cases and the dynamic effects should not be very important because all major chemical processes should be completed at 800°C, we believe that in this case the effects of conduction on one side and convection and radiation on the other probably compensated each other.

From the cumulative pore volume curves of the material CC III in Fig. 1b we can see that there was an about 20–30% increase in the total pore volume after pre-heating to both 600 and 800°C but the character of the curves was not changed dramatically. Nevertheless, a distinct shift towards the bigger pores resulted in the appearance of a significant amount of pores at about 2–3 μm. As the thermal conductivity of specimens pre-heated to 600 and 800°C was in the range of high temperatures higher than of the reference specimens, we have a good reason to believe that in this particular case the convective and radiative effects that are supposedly very distinct in this pore dimension interval probably prevailed the effects of conduction.

High-temperature thermal diffusivity

Figures 13a and b show that the temperature dependences of the thermal diffusivities of both CFRCs exhibit a very similar character to the high-temperature thermal conductivities in Figs 12a and b, concerning both basic $a(T)$ functions and the respective functions of pre-heated samples. The apparent reason is the much more significant dependence of thermal conductivity on temperature compared to both the bulk density and the specific heat capacity.

High-temperature linear thermal expansion coefficient

The linear thermal expansion coefficients of both studied materials are presented in Fig. 14. After a small initial increase with increasing temperature, the $\alpha(T)$ function of the material CC I is rapidly decreasing in the temperature range of 150 to 750°C and then it begins slowly to increase again. The $\alpha(T)$ function of the material CC III is quite different. It first decreases with increasing temperature up to about 330°C, then it increases to about 530°C, and finally it very slowly decreases with temperature in the whole remaining temperature range. Apparently, the differences between the two $\alpha(T)$ curves reflect well the major decomposition processes identified in the DTA curves in Figs 3 and 7.

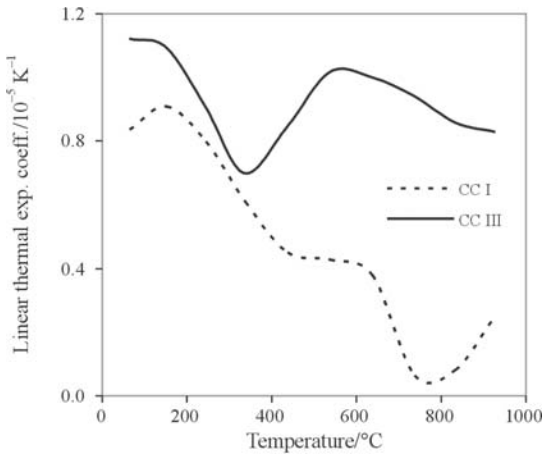

Fig. 14 Linear thermal expansion coefficient of carbon fiber reinforced cement composites CC I, CC III

Comparison with high-temperature thermal properties of cement mortar

The comparison of high-temperature thermal properties of CFRC determined in this paper with those of cement mortar reported in [17] shows that both CC I and CC III resisted to high temperatures much better. The thermal conductivity and thermal diffusivity were lower particularly in the higher temperature range, the linear thermal expansion was lower in the whole temperature range under consideration. This is clearly due to the positive effect of carbon fibers that were able to keep the structure of both materials together even after its damage caused by the thermal decomposition processes.

Conclusions

The measurements of thermal properties of the two different CFRC in high temperature range together with the results of DTA, MIP, SEM and X-ray diffraction analyses in this paper revealed the superior role of the thermal decomposition processes in cement taking place at elevated temperatures. Portland cement is for high-temperature applications generally not very suitable because of the significant mass loss due to the decomposition of $Ca(OH)_2$ at 480–500°C and decomposition of $CaCO_3$ between 740 and 810°C. This mass loss and particularly the local overpressure due to the release of gaseous compounds at relatively high temperatures can lead to a significant damage of the microstructure. In our case the effect of $Ca(OH)_2$ decomposition was reduced significantly by the application of autoclaving process in the specimen production. High alumina cements are more suitable from this point of view in general because they undergo structural changes in the lower temperature range up to about 300°C and the products of the conversion reactions are able to resist to much higher temperatures than the products of decomposition of Portland cement. In the particular case of the measurements in this paper this advantage of high alumina cement was not so pronounced because of the positive effect of the autoclaving process applied in the Portland cement based CFRC production.

It should be noted that the thermal conductivity determined using the solution of inverse problem of transient heat conduction process at one-sided heating as it was done in this paper is rather the apparent thermal conductivity than the thermal conductivity defined by the Fourier's law. The experiment utilized in its measurement is performed in the conditions of large temperature gradients. Therefore, we cannot distinguish exactly between the effects of heat conduction and the effects of convection and radiation. Also, the measurement is dynamic so that any chemical reaction taking place at the elevated temperatures under consideration affects significantly the calculated values of thermal conductivity via the disturbances in the temperature fields due to either the local consumption or release of reaction heat.

The inclusion of other factors than pure heat conduction into the thermal conductivity coefficient certainly decreases the generality of the calculated thermal conductivity *vs.* temperature functions. However, on the other hand it makes possible to perform a very simple assessment of fire resistance of some building structures. For instance, for a dividing structure the most important factor is the time how long it can protect people on its other side from high temperatures. For a fire protecting element of a load-bearing structure the most important factor is the time how long it can protect the underlying, for example steel structure. In the assessment of fire resistance of such structures the knowledge of the apparent thermal conductivity is very beneficial for practical purposes. As in fact it already includes the effects of local heat consumption or release and the effects of convection and radiation, it can be used in simple heat conduction equation instead the Fourier thermal conductivity using exactly the same computer codes.

The knowledge of the dependence of linear thermal expansion coefficient as a function of temperature or just thermal strain as function of temperature is another very useful information for the practice. Together with the known temperature fields that in a structure under fire can be modeled using the simple concept of apparent thermal conductivity it makes possible to perform a thorough stress-strain analysis of such structure. As the dependences of linear thermal expansion coefficients on temperature can be

rather dramatic as it has been shown also in this paper, the increase of accuracy of the calculation of thermal stress comparing to the situation when only the room temperature data of this coefficient are used can be quite remarkable.

Acknowledgements

This research has been supported by the Ministry of Education of the Czech Republic, under contract MSM: 6840770031.

References

1 Y. Ohama, Carbon, 27 (1989) 729.
2 D. D. L. Chung, Carbon Fiber Composites, Butterworth-Heinemann, London 1994.
3 A. Briggs, J. Mater. Sci., 12 (1977) 384.
4 S. B. Park and B. I. Lee, High Temp. – High Press., 22 (1990) 663.
5 P. Soroushian, M. Nagi and A. Alhozaimy, ACI Mater. J., 89 (1992) 131.
6 H. A. Toutanji, T. El-Korchi, R. N. Katz and G. L. Leatherman, Cem. Concr. Res., 23 (1993) 618.
7 T. J. Kim and C. K. Park, Cem. Concr. Res., 28 (1998) 955.
8 A. Katz and A. Bentur, Adv. Cement Based Mater., 3 (1996) 1.
9 X. Fu and D. D. L. Chung, Cem. Concr. Res., 27 (1997) 1799.
10 R. Philleo, J. Am. Concr. Inst., 29/54 (1958) 857.
11 T. Harada, J. Takeda, S. Yamane and F. Furumura, International Seminar on Concrete for Nuclear Reactors. ACI Special Publication No. 34, Vol. 1, Paper SP34-21. American Concrete Institute, Detroit 1972, p. 377.
12 U. Schneider, Behaviour of Concrete at High Temperatures, Ernst and Sohn, Berlin 1982.
13 A. N. Komarovskii, Design of Nuclear Plants, 2nd Edition. Atomizdat, Moscow 1965 (in Russian).
14 T. Z. Harmathy, ASTM J. Mater., 5 (1970) 47.
15 T. Z. Harmathy and L.W. Allen, J. Am. Concr. Inst., 70 (1973) 132.
16 G. Hildenbrand, M. Peeks, A. Skokan and M. Reimann, ENS/ANS Int. Meeting on Nuclear Power Reactor Safety, Vol. 1, Brussels 1978, p. 16.
17 R. Černý, J. Maděra, J. Poděbradská, J. Toman, J. Drchalová, T. Klečka, K. Jurek and P. Rovnaníková, Cem. Concr. Res., 30 (2000) 1267.
18 J. Poděbradská, R. Černý, J. Drchalová, P. Rovnaníková and J. Šesták, J. Therm. Anal. Cal., 77 (2004) 85.
19 W. Roszczynialski, J. Therm. Anal. Cal., 70 (2002) 387.
20 B. Pacewska, I. Wilińska, M. Bukowska, G. Blonkowski and W. Nocuń-Wczelik, J. Therm. Anal. Cal., 77 (2004) 133.
21 E. T. Stepkowska, J. Therm. Anal. Cal., 80 (2005) 727.
22 E. T. Stepkowska, J. M. Blanes, C. Rea and J. L. Perez-Rodriguez, J. Therm. Anal. Cal., 82 (2005) 731.
23 A. Skaropoulou, G. Kakali and S. Tsivilis, J. Therm. Anal. Cal., 84 (2006) 135.
24 Z. P. Bažant and M. F. Kaplan, Concrete at High Temperatures: Material Properties and Mathematical Models, Longman, Harlow 1996.
25 R. Černý and P. Rovnaníková, Transport Processes in Concrete, Spon Press, London 2002.
26 J. Toman and R. Černý, High Temp. – High. Press, 25 (1993) 643.
27 R. Černý and J. Toman, Proc. of International Symposium on Moisture Problems in Building Walls, V. P. de Freitas, V. Abrantes (Eds), Univ. of Porto, Porto 1995, p. 299.
28 J. Toman, P. Koudelová and R. Černý, High Temp. – High Press, 31 (1999) 595.
29 R. Černý, M. Totová, J. Poděbradská, J. Toman, J. Drchalová and P. Rovnaníková, Cem. Concr. Res., 33 (2003) 1347.

Received: September 14, 2006
Accepted: October 3, 2006
OnlineFirst: February 26, 2007

DOI: 10.1007/s10973-006-7944-0